Characterizing perceptual performance at multiple discrimination precisions in external noise

Seong-Taek Jeon,[1,2] Zhong-Lin Lu,[1,*] and Barbara Anne Dosher[3]

[1]*Laboratory of Brain Processes (LOBES), Departments of Psychology and Biomedical Engineering, and Neuroscience Graduate Program, University of Southern California, Los Angeles, California 90089, USA*
[2]*Currently with the Vision Development Lab, Department of Psychology, Neuroscience and Behavior, McMaster University, Hamilton, Ontario, Canada L8S 4K1*
[3]*Memory, Attention, and Perception (MAP) Laboratory, Department of Cognitive Sciences and Institute of Mathematical Behavioral Sciences, University of California, Irvine, Irvine, California 92697, USA*
[*]*Corresponding author: zhonglin@usc.edu*

Received December 18, 2008; revised August 19, 2009; accepted August 27, 2009; posted September 3, 2009 (Doc. ID 104702); published October 5, 2009

Existing observer models developed for studies with the external noise paradigm are strictly applicable only to target detection or identification/discrimination of orthogonal target(s). We elaborated the perceptual template model (*PTM*) to account for contrast thresholds in identifying nonorthogonal targets. Full contrast psychometric functions were measured in an orientation identification task with four orientation differences across a wide range of external noise levels. We showed that observer performance can be modeled by the elaborated *PTM* with two templates that correspond to the two stimulus categories. Sampling efficiencies of the human observers were also estimated. The elaborated *PTM* provides a theoretical framework for characterizing joint feature and contrast sensitivity of human observers. © 2009 Optical Society of America

OCIS codes: 330.0330, 330.4060.

1. INTRODUCTION

Human performance in detection, discrimination, or identification tasks depends on many factors, including stimulus factors such as signal contrast, magnitude, distribution of external noise, and discrimination precision; task factors such as workload, decision structure, and the state of the observer (e.g., attention, fatigue, cognitive factors). However, these factors have mostly been studied in isolation (but see [1]). Perceptual sensitivity, with and without manipulations of task factors, is typically measured in two different ways: (1) as contrast threshold at a particular level of stimulus difference or (2) as feature threshold at a constant (usually high) contrast. Using contrast threshold as the dependent measure, contrast sensitivity studies are usually based on detection of a single stimulus or discrimination of a pair of stimuli with a large and fixed feature difference [e.g., discrimination of two Gabors of ±45°; Fig. 1(a)]. On the other hand, studies using feature threshold as the dependent variable usually keep stimulus contrast at a relatively high level and often involve small feature differences [e.g., discrimination of two 100%-contrast Gabors of $\pm\theta$; Fig. 1(b)]. Examples include the hyperacuity and vernier acuity studies [2–4]. At the theoretical level, virtually all the existing observer models for external noise studies have been developed and tested in the contrast domain, for target detection or identification of orthogonal (or nearly orthogonal) targets [2–6]. In this study, we developed and tested a new form of the perceptual template model (the "elaborated *PTM*," or *ePTM*) to consider identification or discrimination of nonorthogonal targets in high-precision discriminations. This new development provides a quantitative account of feature-difference manipulations and an integrated model for both contrast and feature-difference measurements.

A. Perceptual Sensitivity, Observer Models, and External Noise Methods

Measures of perceptual performance, such as spatial and/or temporal contrast sensitivity functions [7–15] or feature thresholds [16–21] provide the basic building blocks of our understanding of normal and clinical vision. To explain perceptual performance at a more fundamental level, psychophysicists have constructed observer models based on external noise studies that focus on intrinsic limitations of the observer. By separating intrinsic perceptual limitations of the observer from the characteristics of the input stimuli, an observer model provides a framework to generalize results from a particular experiment to predict observer performance in other tasks using different input stimuli but the same observer characteristics [22]. Indeed, it has been shown that many observer characteristics are invariant across different perceptual tasks [22]. This makes the method very useful because it attributes a wide range of limitations in perceptual sensitivity to a few observer limitations.

Behavioral approaches, including many psychological paradigms, have been developed to reveal internal limitations of the perceptual processes and constrain observer models. One major internal limitation, the variability in perceptual processing, is illustrated by inconsistent performance of the observers when they are given the same stimuli multiple times [2,23]. Due to information loss during neural transmission, sampling errors from receptors, random bursts of neuronal spikes, and/or internal varia-

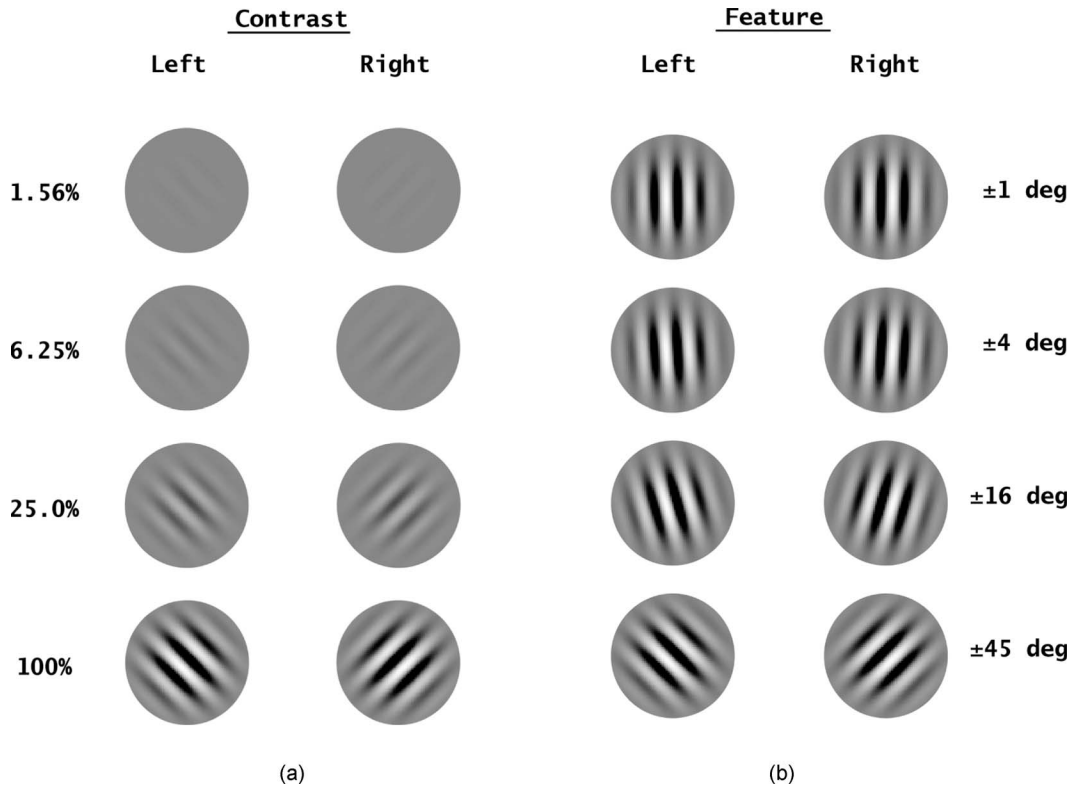

Fig. 1. Examples of a simple Gabor orientation identification task in the (a) contrast and (b) feature domain.

tion of stimulus representation, the variability can be collectively modeled by equivalent internal noises that produce the degree of inefficiency exhibited by the perceptual system [2,5,24–26]. Many behavioral paradigms have been developed to "externalize" the variability of the internal responses by adding external noise to the input stimulus against which to measure the perceptual variabilities. These include various procedures related to critical band masking [27], the equivalent-input noise method [2,4,28–30], the double-pass consistency test [2,23], and the classification-image method [31]. We focus on the equivalent-input-noise method in this article.

1. Equivalent Input Noise Method

The equivalent-input-noise method was originally developed by engineers to measure the intrinsic noise of electronic amplifiers [32–34] and later adopted by sensory psychologists to measure the internal noise of the perceptual system [4,29,30,35] (see [6] for a recent review). The basic idea is that the perceptual system functions like a noisy amplifier, and the internal noise can be estimated by systematically manipulating the magnitude of the external noise superimposed on signal stimuli and measuring threshold-versus-external-noise contrast (*TvC*) functions—signal stimulus energy required for an observer to maintain a certain level of performance as a function of the contrast of the external noise.

The equivalent-input-noise method has been used to reveal internal noise in perceptual processes in a wide range of both auditory [31,36–42] and visual [4,5,24,26,28–30,35,43–52] tasks. The paradigm has also been further developed to investigate mechanisms underlying the effects of various cognitive, developmental, and disease states on the perceptual system [5,6,53–55].

2. Existing Observer Models

Observer models developed for external noise studies, either for target detection or for discrimination or identification of orthogonal (or nearly orthogonal) targets, include the linear amplifier model [4], the induced noise model [2], the linear amplifier model with decision uncertainty [56], the induced noise and uncertainty model [3], and the perceptual template model [5].

In a linear amplifier model (*LAM*), perceptual thresholds are determined by two factors: internal additive noise and observer's sampling efficiency [4,22]. The *LAM* models *TvC* functions at a single performance level, but generally fails to account for *TvCs* at different performance levels [5]. Moreover, estimates of internal additive noise and sampling efficiency from the *LAM* depend on the particular performance criterion level at which contrast thresholds are defined and measured. Various fixes of the *LAM* have been proposed, including the addition of decision uncertainty [56], induced noise [2], both decision uncertainty and induced noise [3], or nonlinear transducer and multiplicative noise [5]. Lu and Dosher [6] conducted a systematic and comprehensive review of the external noise paradigms and all the existing observer models developed to account for performance in external noise studies. They concluded that the five-component *PTM*, with a perceptual template, a nonlinear transducer function, internal additive noise, internal multiplicative noise, and a decision structure, provided the best account

of all the existing data on target detection or discrimination of orthogonal targets in the visual domain.

There has been a significant parallel development of observer models in pattern vision [57–67]. For example, in pattern masking studies, instead of external noise, pattern masks (e.g., sine waves of the same or different frequencies, orientations, etc.) are used to probe the properties of the visual system. Observer models developed and tested in pattern masking studies usually consist of multiple low-level channels and a pooling stage that computes a weighted sum of the outputs of the low-level channels [65–67]. In contrast, observer models developed in external noise studies use a simplified notion, the perceptual template, to represent the overall sensitivity of the perceptual system, corresponding to the weighted contributions of low-level channels in multichannel models, without referring explicitly to the low-level visual channels. The benefits of this formulation are that (1) it relies on very few assumptions about the low-level visual channels, and (2) it uses fewer model parameters to describe a large range of data in external noise studies. The downside is that the formulation makes it difficult to model interactions of low-level visual channels. On the other hand, although they focus on the different properties of the visual system (nonlinearity versus internal noise, interactions of low-level channels versus a global template), the functional forms of some of the observer models in external noise studies and pattern masking studies are very similar (see [6]). In this article, we describe our attempt to elaborate an observer model developed for external noise studies.

3. Ideal Observer Analysis

In this study, data were collected in a Gabor orientation identification task over a wide range of conditions (4 [orientation differences] × 6[external noise levels] × 5[signal contrasts]) for three observers. This large parametric data set gave us an opportunity to use ideal observer analysis to estimate human sampling efficiencies over a wide range of experimental conditions. This was done in three different ways. First, we simulated an ideal observer in all the experimental conditions and estimated sampling efficiencies based on the simulations. These estimated sampling efficiencies depended on the performance level at which contrast threshold was defined because the simulated ideal observer is a linear model that cannot adequately capture the nonlinear properties of the human perceptual processes. To illustrate this point, we performed another ideal observer analysis based on the linear amplifier model, which is essentially an ideal observer model [28]. In the *LAM*, human inefficiencies are attributed to internal additive noise and sampling efficiency relative to the ideal observer. Although traditional ideal observer analysis focuses only on experimental conditions in which external noise is so high that effects of internal noise are ignored, the *LAM*-based analysis includes a wide range of external noise conditions. The method explicitly considers and discounts effects of internal noise on human performance in estimating sampling efficiency. The *LAM*-based ideal observer analysis is consistent with the simulation-based analysis because, like the simulation-based ideal observer analysis, the *LAM*-based ideal observer analysis results in performance-level-dependent sampling efficiency estimates. Finally, we explored the relationship between the *ePTM* and ideal observer analysis. By treating sampling efficiency as a model parameter in the more complex *ePTM*, we obtained performance and task-independent estimates of sampling efficiency for each observer.

B. Overview

The goal of this study is to elaborate the *PTM* to incorporate tasks involving identification or discrimination of nonorthogonal targets. We first describe an experiment that jointly manipulated the magnitude of external noise and the degree of target feature difference. We then present the elaborated *PTM* (*ePTM*) that explicitly considers target feature difference and document its ability to account for the experimental data.

2. EXPERIMENT: *TvC* FUNCTIONS IN A RANGE OF FEATURE DIFFERENCES

Using the method of constant stimuli, we measured full contrast psychometric functions of three observers in an orientation identification task in varying amounts of external noise at fovea. Four orientation differences (±3°, ±6°, ±15°, and ±45° from vertical) were examined, separated in miniblocks in each session across six levels of external noise. Three *TvC* functions, at criterion performance levels of 65, 75, and 85% correct, were estimated in each orientation difference condition.

A. Method

1. Participants

Two naïve observers (CB, JS) and the first author (SJ) participated in the experiment. All observers had corrected-to-normal vision and were experienced in psychophysical studies.

2. Apparatus

The experiment was conducted on a Macintosh Power G4 computer, running MATLAB with Psychtoolbox extensions [69]. All displays were shown on a 17-in. Apple Studio Display monitor with a refresh rate of 120 frames/s. The screen resolution was set to 640 × 480. A special circuit was used to produce a monochromatic signal of high grayscale resolution (>12.5 bits) [70]. Gray levels were linearized using a psychophysical procedure [71]. The available display contrast ranged from −1.0 to 1.0. All displays were viewed binocularly with natural pupils at a distance of approximately 72 cm. A chinrest was used for observers to maintain head position throughout the experiment.

3. Stimuli

The signal stimuli were Gaussian-windowed sinusoidal gratings, oriented ±3°, ±6°, ±15°, and ±45° from vertical. The luminance profile of the Gabor stimuli is described by

$$L(x,y) = L_0(1.0 + c \sin(2\pi f(x \cos\theta + y \sin\theta))\, e^{[-(x^2+y^2)/2\sigma^2]}, \quad (1)$$

where c is the contrast of the Gabor, L_0 is the background luminance, set in the middle of the dynamic range of the display ($L_{min}=1$ cd/m^2; $L_{max}=55$ cd/m^2), $f=1.92$ c/d is the center spatial frequency of the Gabor, and $s=0.52$ deg is the standard deviation of the Gaussian window. The Gabors were rendered on a 64 × 64 pixel grid, extending 2.78° × 2.78° of visual angle.

External noise images were constructed using 2 × 2 pixel elements (0.087° × 0.087°). In every trial, the contrasts of all the noise elements were drawn randomly and independently from the same Gaussian distribution with mean 0 and one of six standard deviations: 0, 0.05, 0.07, 0.12, 0.20, and 0.33. Because the display contrast ranges from −1.0 to 1.0, a sample with standard deviation of 0.33 conforms reasonably well to a Gaussian distribution. Both signal and noise images were centered at fixation.

4. Design

The method of constant stimuli was used to measure *TvC* functions in four Gabor orientation difference conditions (±3°, ±6°, ±15°, and ±45° from vertical). In each external noise condition, the psychometric function for the two-alternative forced-choice identification task was sampled at five signal stimulus contrasts, determined from pilot tests to span the full range of performance levels. There were therefore a total of 4 [orientation differences] × 6 [external noise levels] × 5 [signal contrasts] conditions.

To reduce decision uncertainty, the four orientation difference conditions were run in separate miniblocks of 30 trials each. Within each block, there was one trial from each of the 30 [external noise × signal contrast] conditions. Each experimental session consisted of 40 miniblocks, 10 for each orientation difference condition. The order of trials in each miniblock and the order of miniblocks were both randomized in each session. All observers ran 10 sessions of 1200 trials, for a total of 12,000 trials or 100 trials per experimental condition.

5. Procedure

In the beginning of each miniblock and each trial, observers were reminded of the orientation difference condition by a text string (e.g., "3 deg") in the center of the display. Each trial began after the observer read the string and pressed the space bar on the computer keyboard. This was followed by a display sequence, consisting of a 500 ms fixation cross, a 8.3 ms external noise image, a 8.3 ms signal image, another 8.3 ms independent external noise image, and a blank screen until the end of response, all presented in the center of the monitor. Observers identified the orientation of the Gabor stimulus, using keys "s," "d," or "f" for counterclockwise orientations and "j," "k," or "l" for clockwise orientations. The six keys were used to reduce finger errors; observers generally used "f" and "j." A system beep followed each incorrect response.

B. Results

1. Psychometric Functions

A total of 24 psychometric functions were obtained from each observer, one for each orientation difference and external noise condition (Fig. 2), sampled at five predefined signal contrast levels selected for each external noise condition. Observers exhibited very small overall bias in their choice of the Left/Right responses: 47.5% vs. 52.5%, 51.2% vs. 48.4%, and 50.8% vs. 49.2% for CB, JS, and SJ, respectively.

The psychometric functions were first fitted with the Weibull:

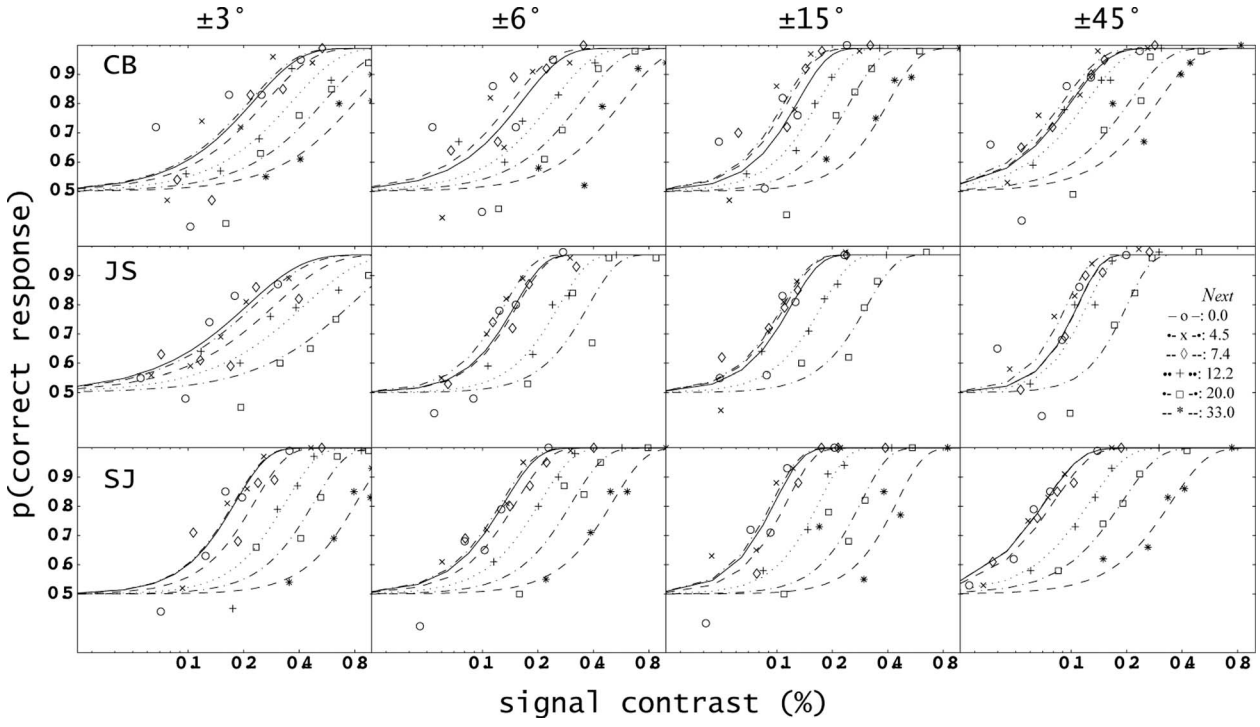

Fig. 2. Full psychometric functions in all the experimental conditions. Smooth curves represent the best fitting Weibull functions.

Table 1. Parameters of the Best-Fitting Weibull Functions

	θ	h	τ_0	τ_1	τ_2	τ_3	τ_4	τ_5	λ	r^2
CB	± 3°	0.585	0.226	0.216	0.266	0.368	0.548	0.815	0.011	0.8006
	± 6°	0.511	0.164	0.164	0.145	0.241	0.346	0.576		
	± 15°	0.372	0.131	0.111	0.116	0.169	0.251	0.407		
	± 45°	0.473	0.101	0.091	0.098	0.122	0.209	0.298		
JS	± 3°	0.697	0.209	0.228	0.294	0.427	0.752	—	0.029	0.8766
	± 6°	0.363	0.150	0.131	0.155	0.261	0.376	—		
	± 15°	0.359	0.120	0.108	0.112	0.176	0.309	—		
	± 45°	0.293	0.109	0.094	0.109	0.122	0.201	—		
SJ	± 3°	0.395	0.181	0.178	0.229	0.338	0.482	0.819	0.001	0.9017
	± 6°	0.405	0.132	0.128	0.153	0.206	0.307	0.509		
	± 15°	0.338	0.098	0.095	0.113	0.170	0.287	0.449		
	± 45°	0.451	0.072	0.072	0.081	0.127	0.189	0.350		

$$P(c) = \xi + (1 - \xi - \lambda)(1 - e^{-(c/\tau)^{\eta}}), \quad (2)$$

where c is the signal contrast, τ is the threshold, η is the slope of the psychometric function, $\xi = 0.5$ represents the chance performance level, and λ represents observer's lapse rate. A maximum-likelihood procedure was used [72]. The *likelihood* is defined as a function of the total number of trials N_i, the number of correct trials K_i, and the percent correct predicted by Eq. (2) in each experimental condition i:

$$likelihood = \prod \frac{N_i!}{K_i!(N_i - K_i)!} P_i^{K_i}(1 - P_i)^{N_i - K_i}, \quad (3)$$

where Π runs across all the experimental conditions for an observer.

Nested-model tests based on χ^2 statistics were used to compare constrained (reduced model) and unconstrained (full model) fits to the psychometric functions:

$$\chi^2(df) = 2 \log\left(\frac{\max likelihood_{full}}{\max likelihood_{reduced}}\right), \quad (4)$$

where $df = k_{full} - k_{reduced}$.

The following constraints were used in fitting the psychometric functions: (1) Each observer has a single lapse rate (λ) across all the orientation difference and external noise conditions. (2) In each orientation difference condition, the psychometric functions in all the external noise conditions have the same slope (η). The Weibull accounted for 80.1%, 87.7%, and 90.2% of the variance for observers CB, JS [73], and SJ, respectively. The constrained psychometric function fits were statistically equivalent to the unconstrained models in which an independent slope value was assumed for each external noise level in each orientation difference condition [$\chi^2(20) = 0.3416$ and 0.3336 for CB and SJ respectively, and $\chi^2(16) = 0.3484$ for JS. $p > 0.90$ for all observers].

The best-fitting Weibull functions are shown as smooth curves in Fig. 2. The parameters of the best-fitting model are listed in Table 1. The lapse rate was very low ($<1.4\%$) across the board. The two most prominent features of the family of psychometric functions are as follows: (1) In each orientation difference condition, the psychometric functions shifted to the right as the external noise increased, and (2) the slope of the psychometric functions increased as the orientation difference increased from ±3° to ±45°.

2. TvC Functions

Contrast thresholds at performance levels of 65%, 75%, and 85% correct, corresponding to d' of 0.5449, 0.9539, and 1.4657, were computed from the best-fitting Weibull functions. The thresholds are plotted as *TvC* functions in each orientation difference condition in Fig. 3. The standard deviation of each threshold was calculated using a re-sampling method [5,74].

The external noise contrast manipulation was highly effective. Averaged across discrimination precision conditions and performance levels, thresholds increased 236%, 177%, and 340% from the zero external noise condition to the highest external noise condition for CB, JS, and SJ, respectively (note: the highest external noise condition for JS is lower than that for CB and SJ). Decreasing orientation difference (and thus increasing the discrimination precision) had two effects on the *TvC* functions. It increased thresholds in all the external noise conditions. Averaged across external noise conditions and observers, thresholds increased 32%, 69%, and 156% from the lowest discrimination precision condition (±45°) to the highest discrimination precision condition (±3°). It also increased the threshold ratio between different performance levels for each external noise condition. Averaged across external noise levels and observers, the threshold ratio between 85% correct and 75% correct performance levels increased from 1.2 to 1.4; the threshold ratio between 75% correct and 65% correct performance levels increased from 1.3 to 1.5. In the following section, we develop an *ePTM* to account for all these effects.

3. MODELING

A. The *ePTM*

Observer models developed for discrimination or identification in external noise assume the existence of a template tuned to each to-be-identified stimulus. The original *PTM* as well as all the other observer models in external

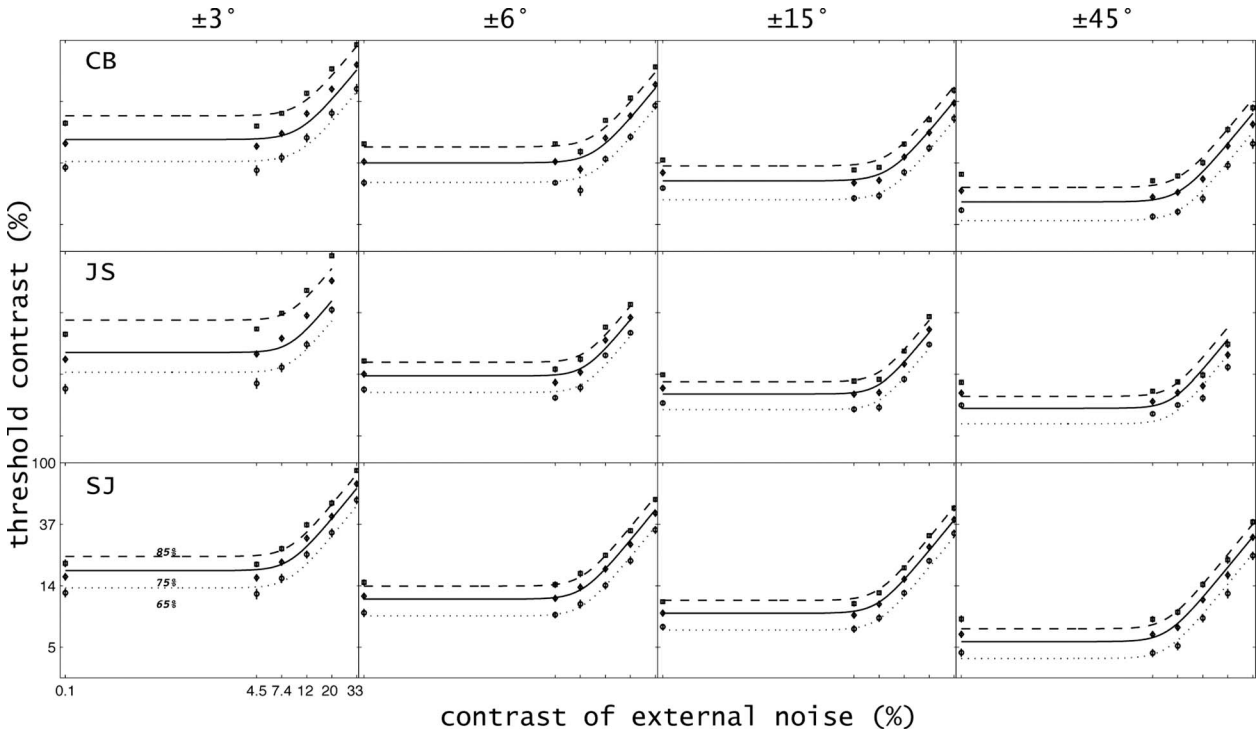

Fig. 3. *TvC* funcitons at 65%, 75%, and 85% performance levels in the four orientation difference conditions. Smooth curves represent the best-fitting *ePTM*. Error bars denote one standard deviation.

noise studies were constructed for cases where any single stimulus plausibly activates only one perceptual template (e.g., Gabors of orientation ±45°). Here, we extended the original *PTM* [5] to include variation in the feature dimension in addition to external noise and signal contrast.

We elaborated the *PTM* based on the results of an extensive analysis of all the major existing observer models developed in external noise studies [6], including the linear amplifier model [4], the induced noise model [2], and the induced-noise-plus-uncertainty model [3]. The *PTM* accommodates all the known "standard" properties of data in external noise experiments. It also provides the best qualitative and quantitative account of a full range of representative data sets.

In the *PTM*, perceptual inefficiencies are attributed to three limitations: internal additive noise that is associated with absolute thresholds in perceptual tasks, internal multiplicative noise that is associated with Weber's law behavior of the perceptual system, and perceptual templates tuned to the target stimuli but that may be broad enough to allow external noise or distracters to affect performance. In the original *PTM* [Fig. 4(a)], the observer is characterized by four parameters: gain to the signal stimulus (β), exponent of the nonlinear transducer function (γ), internal additive noise (N_a), and coefficient of the multiplicative internal noise (N_m). To model two-alternative forced-choice identification or discrimination of nonorthogonal targets, in the [*ePTM*, Fig. 4(b)], we introduce two perceptual templates, one for each of the two stimulus categories. The two templates are assumed to be identical except in the feature dimension under study. In a given trial of a two-alternative forced-choice identification task, a single stimulus is presented and must be identified. The stimulus is better matched to one template $T_B(x,y,t)$ (with gain β_B) and less well matched to the other template $T_W(x,y,t)$ (with gain β_W less than β_B). For example, if two orientations are to be discriminated, two templates are used and a given target stimulus matches one of the templates relatively closely, and—if the two orientations are sufficiently similar—that target stimulus also matches the other template to some degree because the two templates are also relatively similar. We next describe the components of the *ePTM*.

1. Input Stimulus

The model considers input stimuli that include a signal stimulus (i.e., a Gabor of a certain orientation) embedded in white Gaussian external noise. For a signal stimulus with contrast c superimposed with white Gaussian noise images—images made of pixels whose contrasts are samples of jointly independent, identically distributed Gaussian random variables with mean zero and standard deviation N_{ext}—the input stimulus can be expressed as

$$S(x,y,t) = cS_0(x,y,t) + N_{ext}g(x,y,t), \tag{5}$$

where $S_0(x,y,t)$ represents the spatiotemporal pattern of the signal stimulus and $g(x,y,t)$ represents the various contrasts of an external noise image whose value at a particular point (x,y,t) is drawn from a Gaussian distribution with mean 0 and standard deviation 1.0.

2. Template Matching

The input stimulus $S(x,y,t)$ is matched to both templates, $T_B(x,y,t)$ and $T_W(x,y,t)$:

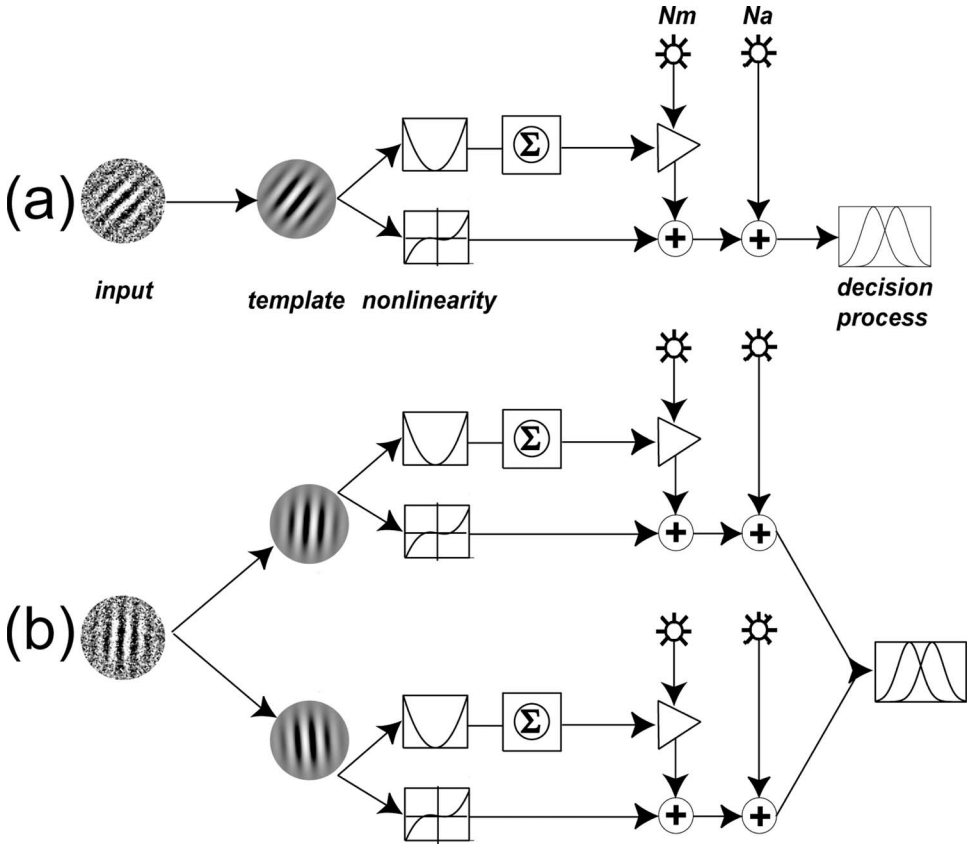

Fig. 4. Schematic representations of the original *PTM* and the *ePTM*. In the *ePTM*, two detectors, one better matched to the signal stimulus in a given trial (with gain β_B) and the less-well-matched to the signal stimulus (with gain β_W), are used to model identification of two nonorthogonal targets.

$$Y_{B1} = \int\int\int T_B(x,y,t)S(x,y,t)\mathrm{d}x\mathrm{d}y\mathrm{d}t$$
$$= c\int\int\int T_B(x,y,t)S_0(x,y,t)\mathrm{d}x\mathrm{d}y\mathrm{d}t$$
$$+ N_{ext}\int\int\int T_B(x,y,t)g(x,y,t)\mathrm{d}x\mathrm{d}y\mathrm{d}t, \quad (6a)$$

$$Y_{W1} = \int\int\int T_W(x,y,t)S(x,y,t)\mathrm{d}x\mathrm{d}y\mathrm{d}t$$
$$= c\int\int\int T_W(x,y,t)S_0(x,y,t)\mathrm{d}x\mathrm{d}y\mathrm{d}t$$
$$+ N_{ext}\int\int\int T_W(x,y,t)g(x,y,t)\mathrm{d}x\mathrm{d}y\mathrm{d}t. \quad (6b)$$

For a given pair of templates and signal stimuli, the values $M_B = \int T_B(x,y,t)S_0(x,y,t)\mathrm{d}x\mathrm{d}y\mathrm{d}t$ and $M_W = \int T_W(x,y,t)S_0(x,y,t)\mathrm{d}x\mathrm{d}y\mathrm{d}t$ are constant; $\int T_B(x,y,t)g(x,y,t)\mathrm{d}x\mathrm{d}y\mathrm{d}t$ and $\int T_W(x,y,t)g(x,y,t)dxdydt$ are Gaussian random variables with mean 0 and a fixed standard deviation σ_{TN}. The outputs from template matching can be rewritten as

$$Y_{B1} = M_B c + N_{ext}\sigma_{TN}\tilde{g}_1(0,1), \quad (7a)$$

$$Y_{W1} = M_W c + N_{ext}\sigma_{TN}\tilde{g}_2(0,1), \quad (7b)$$

where $\tilde{g}_1(0,1)$ and $\tilde{g}_2(0,1)$ are two samples from the standard normal distribution. The two samples may be partially correlated if $T_B(x,y,t)$ and $T_W(x,y,t)$ overlap each other.

3. Nonlinear Transducer

The outputs of the two perceptual templates are then processed by an expansive nonlinear transducer function ($Output = sign(Input)|Input|^{\gamma_1}$), chosen based on similar choices in pattern vision [75,76]. If a stochastic model were fully implemented, nonlinearities (other than 1.0) would require the inclusion of cross products and consideration of the stochastic properties prior to the nonlinearity. This formulation is complex, and in general stochastic models based on Monte Carlo simulations are necessary to model the nonlinear transducer.

In developing the *PTM*, and in order to simplify the task of model estimation and fitting, we introduced analytical simplifications of the stochastic model by using the expectations of the random variables in place of the random variables and ignoring all the cross products. The approach of using analytic simplifications of the full stochastic model in the (analytic) *PTM* has been validated in various ways. First, we (Dosher and Lu [54]) have carried out simulations of the stochastic *PTM* to show that key properties of the analytic *PTM* and mechanisms of state change in the analytic *PTM* are asymptotically consistent

with the stochastic model [77]. Second, the distributional assumptions of the signal detection applications were shown to be approximately true of the stochastic *PTM*. Third, the analytic *PTM* has proven quite robust in accounting for a wide range of data from now dozens of studies that have evaluated not just single conditions but full *TvC* functions at multiple (usually two or three) criterion threshold levels (proxies for the full psychometric functions) [48,54] (see [6] for a review).

We follow the same development in the *PTM* and approximate the outputs of the two detectors after the nonlinear transducer as [78]:

$$Y_{B2} = (M_B c)^{\gamma_1} + N_{ext}^{\gamma_1} \sigma_{TN}^{\gamma_1} F^{\gamma_1}(\gamma_1) \tilde{g}_1(0,1), \tag{8a}$$

$$Y_{W2} = (M_W c)^{\gamma_1} + N_{ext}^{\gamma_1} \sigma_{TN}^{\gamma_1} F^{\gamma_1}(\gamma_1) \tilde{g}_2(0,1), \tag{8b}$$

where $\tilde{g}_1(0,1)$ and $\tilde{g}_2(0,1)$ are two samples from the standard normal distribution. Generally absorbed in later normalization, $F(\gamma_1)$ is a constant that corrects for the effect of nonlinearity on the standard deviation [79].

Because in behavioral studies, the values of M_B, M_W, and $N_{ext}\sigma_{TN}F(\gamma_1)$ can be known only to a constant, without losing any generality we normalized everything relative to $\sigma_{TN}F(\gamma_1)$. This essentially sets $\sigma_{TN}F(\gamma_1)=1$, that is, the total gain of the perceptual templates (integrated over space and time) to 1.0. We define

$$\beta_B = \frac{M_B}{\sigma_{TN}F(\gamma_1)} = \frac{\int\int\int T_B(x,y,t)S_0(x,y,t)\mathrm{d}x\mathrm{d}y\mathrm{d}t}{\sigma_{TN}F(\gamma_1)}, \tag{9a}$$

$$\beta_W = \frac{M_W}{\sigma_{TN}F(\gamma_1)} = \frac{\int\int\int T_W(x,y,t)S_0(x,y,t)\mathrm{d}x\mathrm{d}y\mathrm{d}t}{\sigma_{TN}F(\gamma_1)}, \tag{9b}$$

and rewrite Eqs. (8a) and (8b) as

$$Y_{B2} = (\beta_B c)^{\gamma_1} + N_{ext}^{\gamma_1} \tilde{g}_1(0,1), \tag{8c}$$

$$Y_{W2} = (\beta_W c)^{\gamma_2} + N_{ext}^{\gamma_2} \tilde{g}_2(0,1). \tag{8d}$$

In this formulation, the definition of β_B and β_W depends on $F(\gamma_1)$, which is a function of γ_1. In situations in which a single γ_1 is involved, $F(\gamma_1)$ is just a correction factor on the absolute value of β_B and β_W. In those few situations in which multiple γ_1's are involved, $F(\gamma_1)$ for the different γ_1's must be explicitly considered in the modeling process. Most situations in which the *PTM* has been evaluated involved a single γ_1 [53–55,80,81].

For two templates with gains β_B and β_W, the variations in Y_{B2} and Y_{W2} are partially correlated. When the two templates cease being well approximated as orthogonal and have more overlap, i.e., when β_W is significantly greater than 0, the response to external noise will become more similar as well. We have simulated a stochastic version of the *ePTM* and examined the covariance between the outputs of the two templates after the nonlinear transducer. We found that over a large range of signal contrast levels (0 to 100%), template overlaps (± 1 to ± 45 deg), and γ_1's (1.0 to 3.0), the effective variance of $(Y_{B2} - Y_{W2})$ can be corrected by a factor $\sqrt{1-\beta_w/\beta_B}$: the correction factor accounted for 95.3% of the variance in the simulation study. Therefore, if the perceptual system can utilize the partial correlation of the templates' response to the external noise in decision making, then the effective variance of the external noise should be corrected by a factor of $\sqrt{1-\beta_w/\beta_B}$.

4. Additive and Multiplicative Noise

The model posits that each detector has independent internal additive and multiplicative noise. In both detectors, the additive noise has mean 0 and standard deviation N_a. The variance of the multiplicative noise is a function of the total contrast energy going through each detector. In computing multiplicative noise, the outputs of the two templates are rectified and passed through another nonlinear transducer function ($Output = |Input|^{\gamma_2}$); stimulus energy over a broad range of space, time, and features may be integrated in computing multiplicative noise. The variance of multiplicative noise is proportional to the total stimulus energy in each detector:

$$\sigma_{mB}^2 = N_m^2[N_{ext}^{2\gamma_2} + (\beta_B c)^{2\gamma_2}]. \tag{10a}$$

$$\sigma_{mW}^2 = N_m^2[N_{ext}^{2\gamma_2} + (\beta_W c)^{2\gamma_2}]. \tag{10b}$$

After adding the internal additive and multiplicative noises, the outputs of the two detectors are

$$Y_{B3} = (\beta_B c)^{\gamma_1} + N_{ext}^{\gamma_1}\tilde{g}_1(0,1) + N_a\tilde{g}_3(0,1) + \sigma_{mB}\tilde{g}_5(0,1), \tag{11a}$$

$$Y_{W3} = (\beta_W c)^{\gamma_1} + N_{ext}^{\gamma_1}\tilde{g}_2(0,1) + N_a\tilde{g}_4(0,1) + \sigma_{mW}\tilde{g}_6(0,1), \tag{11b}$$

where $\tilde{g}_3(0,1)$, $\tilde{g}_4(0,1)$, $\tilde{g}_5(0,1)$ and $\tilde{g}_6(0,1)$ are independent samples from the standard normal distribution.

5. Decision

We assume that a difference rule is used at the decision stage. The outputs of the two detectors, Y_{B3} and Y_{W3} are compared:

$$D = Y_{B3} - Y_{W3} = [(\beta_B c)^{\gamma_1} - (\beta_W c)^{\gamma_1}] + N_{ext}^{\gamma_1}[\tilde{g}_1(0,1) - \tilde{g}_2(0,1)] + N_a[\tilde{g}_3(0,1) - \tilde{g}_4(0,1)] + [\sigma_{mB}\tilde{g}_5(0,1) - \sigma_{mW}\tilde{g}_6(0,1)]. \tag{12}$$

In this comparison, the total variance is determined by the variance of all the random variables:

$$\sigma_{total}^2 = 2\sqrt{1-\beta_W/\beta_B}N_{ext}^{2\gamma_1} + N_m^2[2N_{ext}^{2\gamma_2} + (\beta_B c)^{2\gamma_2} + (\beta_W c)^{2\gamma_2}] + 2N_a^2. \tag{13}$$

The average signal-to-noise ratio (d') for the comparison is

$$d' = \frac{mean(Y_{B3}) - mean(Y_{W3})}{\sqrt{\sigma_{total}^2/2}} = \frac{(\beta_B c)^{\gamma_1} - (\beta_W c)^{\gamma_1}}{\sqrt{\sqrt{1-\beta_W/\beta_B}N_{ext}^{2\gamma_1} + N_m^2\left[N_{ext}^{2\gamma_2} + \frac{(\beta_B c)^{2\gamma_2} + (\beta_W c)^{2\gamma_2}}{2}\right] + N_a^2}}. \quad (14)$$

In the special case where $\gamma = \gamma_1 = \gamma_2$, corresponding to the situation where the rising portion of the *TvC* function has a slope of 1.0, we can solve Eq. (14) to obtain threshold signal contrast c_τ as a function of external noise contrast N_{ext} at a given performance criterion (i.e., d'):

$$c_\tau = \left\{ \frac{[(\sqrt{1-\beta_W/\beta_B} + N_m^2)N_{ext}^{2\gamma} + N_a^2]}{\frac{(\beta_B^{2\gamma} - \beta_W^{2\gamma})}{d'^2} - \frac{N_m^2(\beta_B^{2\gamma} + \beta_W^{2\gamma})}{2}} \right\}^{1/2\gamma}. \quad (15)$$

In all the applications of the *PTM* approach so far, we have found that the *PTM* with $\gamma = \gamma_1 = \gamma_2$ has provided adequate descriptions of the empirical data. In the rest of this article, we will restrict our discussion to this simplified set of *PTM*s. The same logic could be followed to understand the properties of *PTM*s with $\gamma_1 \neq \gamma_2$.

It follows directly from Eq. (15) that for any given external noise contrast $\forall N_{ext}$, the threshold signal contrast ratio between two performance criterion levels (corresponding to d_2' and d_1'), is

$$\frac{c_{\tau_2}}{c_{\tau_1}} = \left[\frac{\frac{(\beta_M^{2\gamma} - \beta_U^{2\gamma})}{d_1'^2} - \frac{N_m^2(\beta_M^{2\gamma} + \beta_U^{2\gamma})}{2}}{\frac{(\beta_M^{2\gamma} - \beta_U^{2\gamma})}{d_2'^2} - \frac{N_m^2(\beta_M^{2\gamma} + \beta_U^{2\gamma})}{2}} \right]^{1/2\gamma}. \quad (16)$$

Thus, the *ePTM* predicts that threshold signal contrast ratio between two performance criterion levels in any external noise contrast condition is a nonlinear function of the corresponding d', independent of the particular external noise level. These ratios are predicted to be independent of the external noise contrast (a testable model property) and form one competitive basis for favoring the *PTM* over alternative observer models. A full specification of all the parameters of an *ePTM* requires measurement of *TvC* functions at three (or more) separate levels of feature differences at each of three (or more) performance levels.

6. Relationship to LAM and Ideal Observer Analysis

The *ePTM* is elaborated from the *LAM* by incorporating additional processing of the stimulus and noise, including the nonlinear transducer, and multiplicative noise. If we set $\gamma = 1$, $N_m = 0$, and $\beta_W = 0$, the *ePTM* is "reduced" to the *LAM*, and Eq. (15) becomes

$$c_\tau = \left[\frac{d'^2}{\beta_B^2}(N_{ext}^2 + N_a^2) \right]^{1/2}. \quad (17)$$

The *LAM* was developed as a form of an ideal observer model. If we square both sides of Eq. (17), we have

$$c_\tau^2 = \frac{d'^2}{\beta_B^2}(N_{ext}^2 + N_a^2). \quad (17b)$$

Because β_B reflects signal gain of the human observer, we can reformulate it in terms of the gain β_{IB} of the ideal observer and sampling efficiency v:

$$\beta_B = \sqrt{v}\beta_{IB}. \quad (18)$$

Substituting Eq. (18) into Eq. (17b), we obtain the efficiency-based formulation of the *LAM* [26]:

$$c_\tau^2 = \frac{d'^2}{v\beta_{IB}^2}(N_{ext}^2 + N_a^2) = \frac{1}{vk}(N_{ext}^2 + N_a^2), \quad (17c)$$

where $k = \beta_{IB}^2/d'^2$. If the slope of the *TvC* function is a, then the efficiency is

$$v = \frac{1}{ak} = \frac{d'^2}{a\beta_{IB}^2}. \quad (19)$$

Equation (19) allows one to estimate *LAM* sampling efficiency from the slope of the threshold versus external noise functions. Although traditional ideal observer analysis focuses only on experimental conditions in which external noise is so high that the contributions of internal noise can be ignored, the *LAM* analysis includes a wide range of external noise conditions. The method explicitly considers and discounts effects of internal noise on human performance in the computation of efficiency.

This reformulation of the *LAM* also illustrates the relationship of the *ePTM* to ideal observer analysis and indicates in a parallel development how to estimate sampling efficiency through the *ePTM*. Essentially, we can reformulate β_B in terms of the gain β_{IB} of the ideal observer and sampling efficiency of the human observer v:

$$\beta_B = \sqrt{v}\beta_{IB}. \quad (20)$$

In simple detection tasks, the template of the ideal observer is matched to the signal stimulus. In identification or discrimination tasks, the template of the ideal observer is matched to the signal stimulus—which then yields an ideal computation if the decision rule is ideal [82,83]. We can apply Eq. (9) to the actual stimuli used in the experiments to compute the gain of the ideal observer.

Although other components of the *ePTM*, the nonlinear transducer, multiplicative noise, and the gain of the less-well-matched template also affect human performance, our approach here is to model them explicitly in the *ePTM* and discount their contributions in estimating human sampling efficiency, just as additive noise is explicitly considered and discounted in the *LAM*-based ideal observer analysis.

Table 2. Parameters of the Best-Fitting *ePTM*

	CB	JS	SJ
β_B	1.062	0.8290	1.075
$\beta_W \pm 3°$	0.9486	0.7620	1.023
$\pm 6°$	0.8515	0.6921	0.9387
$\pm 15°$	0.6966	0.5447	0.8458
$\pm 45°$	0	0	0
N_m	0.1047	0.1170	0.0261
N_a	0.0098	0.0024	0.0031
γ	1.818	2.216	2.050
r^2	0.9749	0.9335	0.9890
$F(6,59)$	0.123	0.017	0.019
$F(3,62)$	0.000	0.000	0.000
$F(3,62)$	0.257	0.092	0.042

4. EVALUATING THE *ePTM*

To evaluate the *ePTM* using the current parametric data set, we tested whether a single model with only β_W varying as a function of orientation difference can fit all the *TvC* functions in all the experimental conditions (with $\beta_W=0$ in the ± 45 condition). The model includes seven parameters: shared N_a, N_m, γ, and β_B across the orientation difference conditions, and three β_W's for the ± 3, ± 6, and ± 15 deg conditions of the experiment. Fits of this most reduced seven-parameter model to the data were compared with three more saturated models, including (1) two models with 10 parameters that allowed N_a or N_m, in addition to β_W, free to vary in the four orientation difference conditions and (2) one model with 13 parameters that allowed both N_a and N_m free to vary in the four orientation difference conditions. In fitting the *ePTM*, the standard deviation of external noise was multiplied by $\sqrt{2}$ to reflect the use of two independent external noise frames in each trial.

A least-square procedure with the following cost function,

$$RSS = \sum [\log(c_\tau^{predicted}) - \log(c_\tau^{measured})]^2, \quad (21)$$

where $c_\tau^{predicted}$ is computed using Eq. (15), and Σ represents summation across three performance levels of all the external noise and orientation difference conditions for an observer, was used to search for the best fitting parameters of each model. The goodness of model fits was gauged by

$$r^2 = 1.0 - \frac{\sum [\log(c_\tau^{predicted}) - \log(c_\tau^{measured})]^2}{\sum [\log(c_\tau^{measured}) - mean(\log(c_\tau^{measured}))]^2}, \quad (22)$$

where Σ and mean () run across all the experimental conditions for an observer. An *F*-test for nested models was used to statistically compare the models. For two nested models with k_{full} and $k_{reduced}$ parameters, the *F* statistic is defined as

$$F(df_1, df_2) = \frac{(r_{full}^2 - r_{reduced}^2)/df_1}{(1 - r_{full}^2)/df_2}, \quad (23)$$

where $df_1 = k_{full} - k_{reduced}$, and $df_2 = N - k_{full}$; N is the number of predicted data points.

The most reduced model, which only allows β_W free to vary across discrimination precision conditions, accounted for 97.4%, 93.3%, and 98.9% of the variance for CB, JS, and SJ, respectively. For all three observers, allowing N_a and/or N_m free to vary across the four orientation difference conditions did not significantly improve the fits (all $p > 0.25$). We conclude that the most reduced model in which the gain of the less-well-matched template varies as a function of orientation difference provides the best account of the *TvC* functions. The parameters of the best-fitting model are listed in Table 2.

In Fig. 5, we plotted the average β_W/β_B of the best-fitting model of the three observers as a function of the orientation difference. If we assume that across the four orientation difference conditions, only the overlap between the better matched and less-well-matched tem-

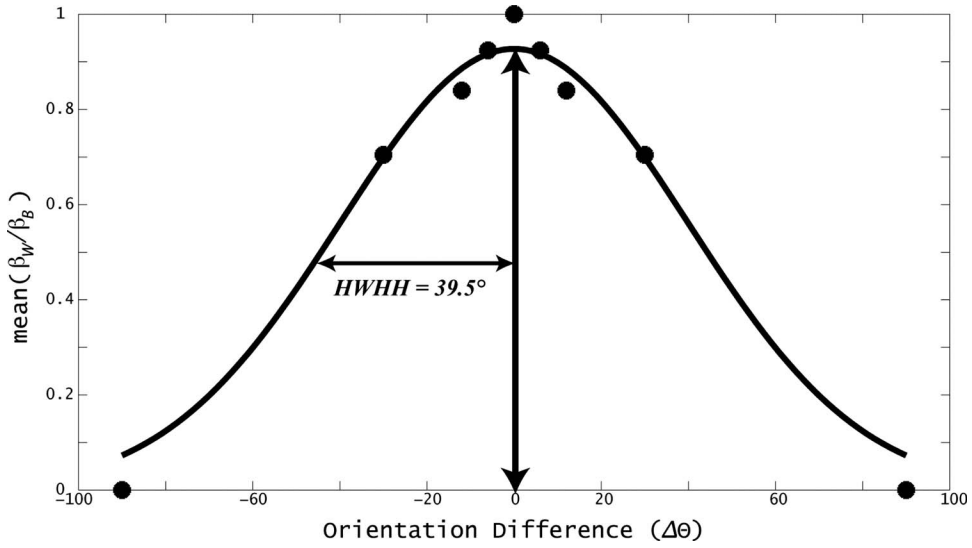

Fig. 5. Schematic representation of the perceptual template based on normalized β_W.

plates changes but the shapes of the perceptual template remains the same and can be modeled as a Gaussian, we can estimate the bandwidth of the perceptual template by fitting a Gaussian to the data in Fig. 5. The resulting half-width bandwidth at half-height is 39.5°.

The *ePTM* without the correction factor of the covariance of the outputs of the two perceptual templates in each orientation difference condition was also evaluated. Although estimates of the model parameters are slightly different, the general qualitative results did not change.

5. IDEAL OBSERVER ANALYSIS

A. Simulation-Based Analysis

The performance of an ideal observer was simulated using the stimuli and tasks in the experiment, with the assumption that the ideal observer has an integration window that is at least 25 ms, which is the duration of the stimulus in each trial of the experiment. The *TvC* functions at three performance levels (65%, 75%, and 85% correct) for the ideal observer are plotted in Fig. 6 as squared contrast threshold c^2_{ideal} versus the variance of the external noise functions. A linear function,

$$c^2_{Ideal}(Pc|task) = \mu_{Ideal}(Pc|task)N^2_{ext}. \quad (24)$$

provided an excellent account of these *TvC* functions (r^2 =0.9999). The slopes of the *TvC* functions $\mu(Pc|task)$ for the four orientation difference conditions at 65%, 75%, and 85% correct performance levels are listed in Table 3.

We also replotted the *TvC* functions of the human observers in terms of squared contrast thresholds versus external noise variance in Fig. 6. Again, the variance of the external noise was corrected by a factor of 2 to reflect the use of two independent external noise frames in each trial. A linear regression analysis was used to extract the slopes and intercepts of the human *TvC* functions

$$c^2_{Human}(Pc|task,obs) = \mu_{Human}(Pc|task,obs)N^2_{ext} + b. \quad (25)$$

The linear equation [Eq. (25)] provided excellent account of the human data, accounting for 99.8%, 99.3%, and 99.8% variance for CB, JS, and SJ, respectively. The slopes and intercepts are listed in Table 3.

We then calculated the sampling efficiencies of the human observers using the following definition [28]:

$$\nu(Pc|task,obs) = \frac{\mu_{Ideal}(Pc|task)}{\mu_{Human}(Pc|task,obs)}. \quad (26)$$

The results are listed in Table 4.

For the three observers in this study, sampling efficiencies ranged from 0.018 to 0.098. In a given orientation difference condition, the estimated sampling efficiency increased with performance level. For example, for observer CB, sampling efficiency = 0.035, 0.050, and 0.066 at 65%, 75%, and 85% correct performance levels, respectively, in the ±45 deg condition. The dependence of the estimated sampling efficiency on the performance level reflects a major shortcoming of the conventional ideal observer analysis, which uses a linear model to estimate properties of the often nonlinear perceptual processes. We further discuss this point in the next section.

B. *LAM*-Based Analysis

The *LAM* predicts a linear relationship between squared contrast threshold and the variance of external noise. For nonoverlapping stimulus categories (±45 deg), ideal observer analysis based on the efficiency-based formulation

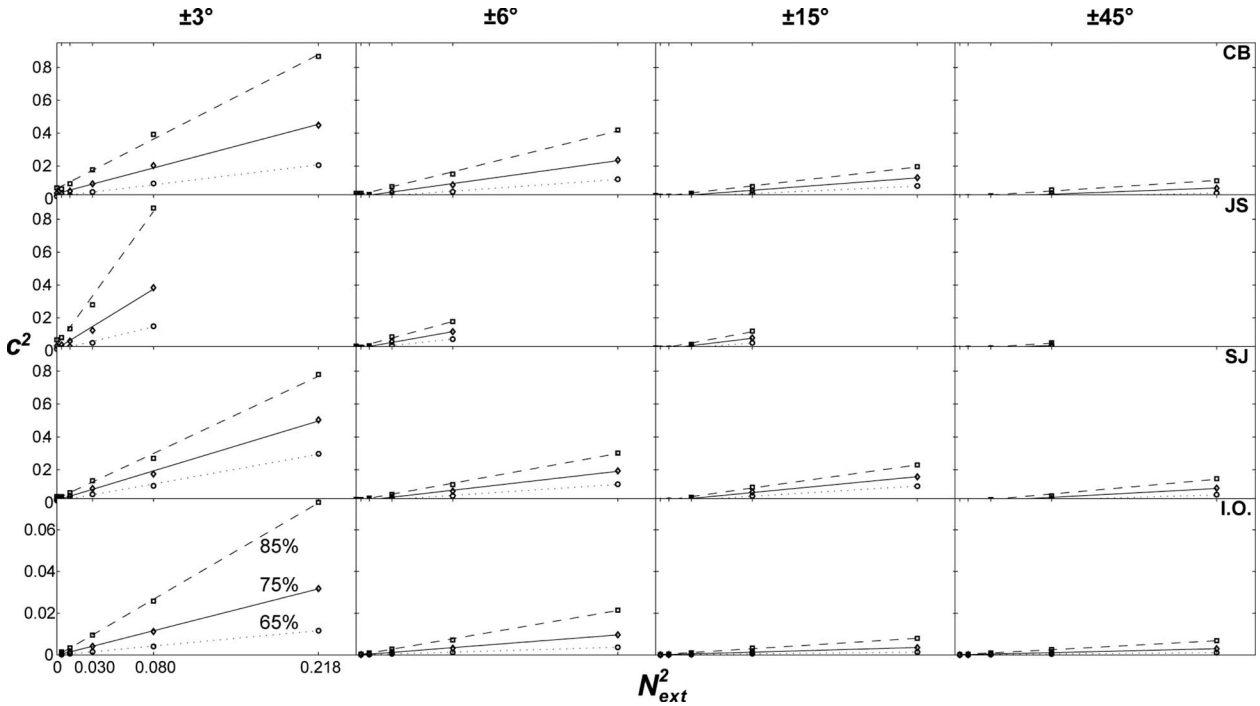

Fig. 6. *TvC* functions at 65%, 75%, and 85% performance levels in the four orientation difference conditions, plotted as squared contrast thresholds versus variance of external noise for the three human observers (first three rows) and the ideal observer (last row). The lines represent the results of the linear regression analysis.

Table 3. Slopes and Intercepts of the Squared Threshold Contrast versus External Noise Variance Functions

Observer	Percent Correct (%)	Orientation Separation ($\Delta\theta$) ± 3° Slope	± 3° Intercept	± 6° Slope	± 6° Intercept	± 15° Slope	± 15° Intercept	± 45° Slope	± 45° Intercept
CB ($r^2=0.9975$)	65	0.88	0.015	0.51	0.006	0.34	0.005	0.15	0.003
	75	1.94	0.032	1.02	0.011	0.55	0.007	0.28	0.006
	85	3.75	0.062	1.81	0.020	0.84	0.011	0.47	0.009
JS ($r^2=0.9928$)	65	1.74	0.005	0.79	0.008	0.54	0.003	0.22	0.005
	75	4.48	0.014	1.30	0.012	0.88	0.005	0.32	0.007
	85	10.14	0.032	1.98	0.019	1.34	0.008	0.46	0.010
SJ ($r^2=0.9976$)	65	1.31	0.009	0.49	0.005	0.45	0.003	0.22	0.000
	75	2.21	0.016	0.84	0.008	0.71	0.005	0.39	0.001
	85	3.42	0.024	1.31	0.013	1.03	0.007	0.65	0.001
IO ($r^2=0.9999$)	65	0.053	0	0.017	0	0.0061	0	0.0051	0
	75	0.146	0	0.044	0	0.0163	0	0.0137	0
	85	0.336	0	0.099	0	0.0366	0	0.0312	0

of the *LAM* [Eq. (17c)] is identical to the simulation-based ideal observer analysis. We calculated β_{IB} [Eq. (9)] by using two ideal templates that are completely matched to the ±45 deg Gabor stimuli and the exact signal and external noise images used in the study. Because very brief (8.3 ms) external noise and Gabor image frames were used, perfect summation was assumed in the calculation. The result is $\beta_{IB}=8.05$. The d' values corresponding to 65%, 75%, and 85% correct performance are 0.5449, 0.9539, and 1.4657. The sampling efficiencies were calculated from the slopes of the *TvC* functions using Eq. (19). For CB, sampling efficiency is 0.032, 0.051, and 0.069 at the 65%, 75%, and 85% correct performance levels, respectively. For JS, sampling efficiency is 0.022, 0.044, and 0.072 at the three performance levels. For SJ, sampling efficiency is 0.022, 0.036, and 0.050 at the three performance levels. These values are very similar to those obtained from the simulation-based ideal observer analysis and comparable to estimated sampling efficiencies in the literature [51,84,85].

Like the estimated sampling efficiencies from the simulation-based ideal observer analysis, the estimated sampling efficiencies from the *LAM*-based ideal observer analysis varied with performance level. This suggests that both the simulation-based and the *LAM*-based efficiency estimates are not self-coherent. According to the *LAM*, the ratio between the slopes and intercepts at two different performance levels is equal to the corresponding d'^2 ratios. The d'^2 ratios between 75% and 65% correct, and between 85% and 75% correct are 3.06 and 2.36, respectively. For the human observers, the relationship between the slopes and intercepts at different performance levels are, however, inconsistent with the predictions of the *LAM* ($p<0.005$). For our observers, the average ratio of *TvC* slopes between the 75% and 65% correct and between 85% and 75% correct performance levels are 1.73 and 1.59 in the ±45 deg condition. Very similar ratios are also obtained for the intercepts. That the observed slope and intercept ratios are much lower than the corresponding d'^2 ratios confirms our earlier findings that the *LAM*

Table 4. Sampling Efficiencies of the Human Observers

Efficiency	Performance	± 3°	± 6°	± 15°	± 45°
v_i (CB)	65%	0.061	0.033	0.018	0.035
	75%	0.076	0.044	0.030	0.050
	85%	0.090	0.055	0.044	0.066
v_i (JS)	65%	0.031	0.021	0.011	0.024
	75%	0.033	0.034	0.019	0.042
	85%	0.033	0.050	0.027	0.069
v_i (SJ)	65%	0.041	0.035	0.014	0.024
	75%	0.066	0.053	0.023	0.035
	85%	0.098	0.075	0.036	0.048

is not consistent with the observed threshold ratios between different performance levels (see [6] for a review). This is a parallel observation to what was previously made on threshold ratios [5,6]. Increased sampling efficiency with performance level is, however, consistent with predictions of observer models that incorporate decision uncertainty [3,56], template learning [86], or transducer nonlinearity [5].

C. *ePTM*-based Efficiency Estimation

In contrast to the *LAM*, the *ePTM* provided an excellent account of observer performance over a wide range of performance levels in this study. Formulating the *ePTM* with an application parallel to the *LAM* to understand sampling efficiency within the context of other perceptual inefficiencies such as nonlinear transducer and multiplicative noise provides a coherent framework for comparing human performance to ideal observer performance.

It is assumed that the optimal template for each stimulus is a matched filter, and that the decision rule (here, the difference rule, which is equivalent to a *max* rule in this case) is also optimal. Using the actual signal and external noise stimuli used in the study, we computed β_{IM} =6.10 [Eq. (9)]. From the values of β_B's of the best-fitting *ePTM*, the estimated sampling efficiency, which accounts for performance in all three criteria, is 0.030, 0.019, and 0.031 for CB, JS, and SJ, respectively.

In the *ePTM*-based ideal observer analysis, we treated sampling efficiency as a model parameter in the more complex *ePTM* and estimated it in the context of the model. This yields a single, consistent sampling efficiency across all the performance levels and experimental conditions for each observer.

6. DISCUSSION

All the existing observer models for external noise studies have been developed in the context of target detection or discrimination or identification of orthogonal (or nearly orthogonal) targets. In this study, we elaborated and tested a new form of the perceptual template model, the "*ePTM*," to consider identification or discrimination of nonorthogonal targets required in high-precision discriminations, as well as the treatment of feature difference thresholds. Using the method of constant stimuli, we collected full contrast psychometric functions from three observers in an orientation identification task at fovea in four orientation difference conditions (±3°, ±6°, ±15°, and ±45° from vertical) and across a wide range of external noise levels. We showed that the families of *TvC* functions in the four orientation difference conditions exhibited some very regular properties. The simplest elaboration of the *PTM*, with the same template gain to the better matched signal stimulus (β_B), nonlinearity (γ), internal additive noise (N_a), and coefficient for multiplicative noise (N_m) but varying gains of the less-well-matched template (β_W) across the orientation difference conditions, provided the best fit to all the data, accounting for 93.3%–98.9% of the variance. Sampling efficiencies of human observers were also estimated from the best-fitting *ePTM*.

From the gains of the perceptual templates in different orientation difference conditions, we found that the perceptual templates are broadly tuned in orientation: the orientation bandwidth of the perceptual template is about 39.5° and there is considerable overlap between the templates in relatively high discrimination precision conditions. Based on Fourier analysis, the half-height half-width of the Gabor signal used in this study is 39.5°. The estimated orientation bandwidth of the perceptual template matches very well that of the Gabor stimuli. The close match of the orientation bandwidth of the perceptual template with that of the Gabor stimuli suggests that observers used near-optimal weights of the visual information in the stimulus, supporting the notion of matched filters in visual recognition [87,88]. However, their sampling efficiencies were very low. Similar results have been obtained by others [89].

The estimated bandwidth of the perceptual template in the current psychophysical study reflects the orientation bandwidth at the overall observer level. It is much broader than that of single neurons in early visual cortical areas [90,91]. For example, the average tuning width for orientation was about 14° in a single cell study of cat cortex [92]. Another study by Campbell and Kulikowski [93] also found that the masking effect of one grating on another differed in orientation by approximately 12°–15°. On the other hand, a good deal of psychophysics research [75,76,82,94–96] has demonstrated that the human visual system is exquisitely sensitive to the orientation of lines or gratings. For example, in a line orientation identification task, Westheimer [96] found that the best thresholds are around 0.2°–0.8° [85], 0.4°–0.8° [97], and 0.17°.

Several approaches have been proposed to resolve the apparent discrepancy between broad orientation tuning of cortical neurons (10°–20°) and acute human orientation discrimination threshold (0.2°–0.8°) [18,76,85,98,99]. For example, Geisler [76] proposed an ideal detector model based on retinal signal and the cone sampling mosaic of the retina for a hyperacuity task. Westheimer *et al.* [99] assumed that, while detection is determined by the most excited orientation-tuned neural element, the sharpness of suprathreshold orientation discrimination is determined by the relative activities of two or more broadly tuned orientation-sensitive neural elements signaling the difference among those activities. This idea has been framed in both the opponent-process [98] and line-element [100,101] formulations. These two formulations share the same idea that orientation discrimination is not limited by the bandwidth of the broadly selective neural elements but by a combination of their noise levels and the shape of their sensitivity curves (specifically, by the maximum slope difference). Regan and Beverly [98] made a clear demonstration that a detector that is most sensitive for detecting faint stimuli near its preferred orientation contributes either almost nothing or mere noise to the discrimination of subtle orientation differences around its preferred orientation (since the width of the orientation tuning curve is broad). They proposed that one possible way to discriminate these orientations is to compare relative responses from neighboring detectors. The idea was supported by Waugh *et al.* [95], who found a bimodal curve with distinct peaks at about 10° on either

side of the center line orientation in a vernier task masked by one-dimensional visual noise. The idea has also found support in physiological research [92,102]. For example, Bradley *et al.* [92] measured the minimum difference in stimulus orientation and spatial frequency that can produce reliable changes in the response of individual neurons in cat visual cortex. They compared these values with those obtained from behavioral thresholds reported in other experiments. Although the average minimum orientation difference that could be signaled reliably by most cells from their sample was 6.4°, which was well above the behaviorally determined thresholds, they reported that the most selective cells signaled orientation differences as small as 1.84°, which are comparable in magnitude to the behaviorally observed thresholds. Most notably, the slope was reduced, and the variability was maximal near the peak of the tuning function. Therefore, Bradley and colleagues [92] concluded that neurons that respond most sensitively to a particular stimulus provide little information about orientation changes in the vicinity of the stimulus. All these results implicate that the mechanisms most sensitive to a minute offset or difference of features are processors (templates, cells, or filters) at orientations neighboring the mechanisms that detect the target.

The *ePTM* belongs to the general class of psychophysical models that use rather broadly tuned perceptual processors to achieve high discrimination precision. In the *ePTM*, visual stimuli are first processed by perceptual templates that are tuned to the stimuli in the dimension of variation. The overlap between the better-matched and the less-well-matched perceptual templates determines the discrimination precision. The *ePTM* extends the earlier models by considering nonlinearities and internal noise sources of the observer and is capable of modeling full psychometric functions over a wide range of external noise levels and orientation differences.

The *ePTM* also provides an alternative framework to estimate sampling efficiencies of human observers. Traditionally, ideal observer analysis is based only on the statistical properties of the input stimulus without any consideration of the perceptual process [50,84]. In this study, conventional simulation-based ideal observer analysis resulted in performance-dependent estimates of sampling efficiencies, because the conventional ideal observer analysis is based on linear models that cannot adequately capture nonlinear properties of the perceptual processes. By taking into account the internal additive noise, the *LAM*-based ideal observer analysis allows us to separate the contributions of internal additive noise from sampling efficiency [26]. The *ePTM*-based ideal observer analysis pursues this important direction. By incorporating additional observer inefficiencies other than sampling efficiency, the *ePTM*-based ideal observer analysis provides an excellent account of human performance as well as coherent estimates of sampling efficiencies.

The elaborated *PTM* provides an integrated framework within which to understand the performance limitations of the observer in the two fundamental measurement regimes of contrast thresholds and feature thresholds. Within the new elaborated observer framework, we can characterize human performance in the "perceptual space"—human performance as a joint function of external noise and feature difference. This in turn will allow us to address the question of mechanisms associated with observer state changes (e.g., attention, perceptual learning) in a wide range of tasks involving different manipulations of task difficulty (achievable accuracy), including both the contrast threshold and feature threshold regimes.

ACKNOWLEDGMENTS

The research was supported by the National Eye Institute (NEI), EY017491, and the National Institute of Mental Health (NIMH), MH081018. We thank Bosco Tjan for discussing the ideal observer analysis with us.

REFERENCES AND NOTES

1. L. Itti, C. Koch, and J. Braun, "Revisiting spatial vision: toward a unifying model," J. Opt. Soc. Am. A **17**, 1899–1917 (2000).
2. A. E. Burgess and B. Colborne, "Visual signal detection. IV. Observer inconsistency," J. Opt. Soc. Am. A **5**, 617–627 (1988).
3. M. P. Eckstein, A. J. Ahumada, and A. B. Watson, "Visual signal detection in structured backgrounds. II. Effects of contrast gain control, background variations, and white noise," J. Opt. Soc. Am. A **14**, 2406–2419 (1997).
4. D. Pelli, "Effects of visual noise," Ph.D. dissertation (Cambridge Univ. 1981).
5. Z.-L. Lu and B. A. Dosher, "Characterizing human perceptual inefficiencies with equivalent internal noise," J. Opt. Soc. Am. A **16**, 764–778 (1999).
6. Z. L. Lu and B. A. Dosher, "Characterizing observers using noise and observer models: assessing internal representations with external noise," Psychol. Rev. **115**, 44–82 (2008).
7. D. H. Kelly, "Spatial frequency selectivity in the retina," Vision Res. **15**, 665–672 (1975).
8. D. H. Kelly, "Motion and vision. II. Stabilized spatio-temporal threshold surface," J. Opt. Soc. Am. **69**, 1340–1349 (1979).
9. J. J. Koenderink, M. A. Bouman, A. E. Bueno de Mesquita, and S. Slappendel, "Perimetry of contrast detection thresholds of moving spatial sine wave patterns. IV. The influence of the mean retinal illuminance," J. Opt. Soc. Am. **68**, 860–865 (1978).
10. A. B. Watson, "Estimation of local spatial scale," J. Opt. Soc. Am. A **4**, 1579–1582 (1987).
11. J. Rovamo and V. Virsu, "An estimation and application of the human cortical magnification factor," Exp. Brain Res. **37**, 495–510 (1979).
12. J. Rovamo, V. Virsu, and R. Nasanen, "Cortical magnification factor predicts the photopic contrast sensitivity of peripheral vision," Nature **271**, 54–56 (1978).
13. G. T. Plant, "Temporal properties of normal and abnormal spatial vision," in *Spatial Vision*, D. Regan, ed. (CRC Press, 1991), pp. 43–63.
14. D. Regan, "Spatiotemporal abnormalities of vision in patients with multiple sclerosis," in *Spatial Vision*, D. Regan, ed. (CRC Press, 1991), pp. 239–249.
15. R. F. Hess and E. R. Howell, "The threshold contrast sensitivity function in strabismic amblyopia: evidence for a two type classification," Vision Res. **17**, 1049–1055 (1977).
16. J. P. Thomas and J. Gille, "Bandwidths of orientation channels in human vision," J. Opt. Soc. Am. **69**, 652–660 (1979).
17. V. Virsu and J. Rovamo, "Visual resolution, contrast sensitivity, and the cortical magnification factor," Exp. Brain Res. **37**, 475–494 (1979).

18. B. C. Skottun, A. Bradley, G. Sclar, I. Ohzawa, and R. D. Freeman, "The effects of contrast on visual orientation and spatial frequency discrimination: a comparison of single cells and behavior," J. Neurophysiol. **57**, 773–786 (1987).
19. B. G. Smith and J. P. Thomas, "Why are some spatial discriminations independent of contrast?" J. Opt. Soc. Am. A **6**, 713–724 (1989).
20. S. F. Bowne, "Contrast discrimination cannot explain spatial frequency, orientation or temporal frequency discrimination," Vision Res. **30**, 449–461 (1990).
21. P. Vazquez, M. Cano, and C. Acuna, "Discrimination of line orientation in humans and monkeys," J. Neurophysiol. **83**, 2639–2648 (2000).
22. D. G. Pelli and B. Farell, "Why use noise?" J. Opt. Soc. Am. A **16**, 647–653 (1999).
23. D. M. Green, "Consistency of auditory detection judgments," Psychol. Rev. **71**, 392–407 (1964).
24. J. A. J. Ahumada and A. B. Watson, "Equivalent-noise model for contrast detection and discrimination," J. Opt. Soc. Am. A **2**, 1133–1139 (1985).
25. L. Kiorpes and J. A. Movshon, "Peripheral and central factors limiting the development of contrast sensitivity in Macaque monkeys," Vision Res. **38**, 61–70 (1998).
26. D. G. Pelli, "The quantum efficiency of vision," in *Vision: Coding and Efficiency*, C. Blakemore, ed. (Cambridge Univ. Press, 1990), pp. 3–24.
27. H. Fletcher, "Auditory patterns," Rev. Mod. Phys. **12**, 47–65 (1940).
28. H. B. Barlow, "Retinal noise and absolute threshold," J. Opt. Soc. Am. **46**, 634–639 (1956).
29. G. E. Legge, D. Kersten, and A. E. Burgess, "Contrast discrimination in noise," J. Opt. Soc. Am. A **4**, 391–404 (1987).
30. N. S. Nagaraja, "Effect of luminance noise on contrast thresholds," J. Opt. Soc. Am. **54**, 950–955 (1964).
31. A. J. Ahumada and J. Lovell, "Stimulus features in signal detection," J. Acoust. Soc. Am. **49**, 1751–1756 (1971).
32. H. T. Friis, "Noise figures of radio receivers," Proc. IRE **32**, 419–422 (1944).
33. W. W. Mumford and E. H. Schelbe, *Noise Performance Factors in Communication Systems* (Horizon House-Microwave Inc., 1968).
34. D. O. North, "The absolute sensitivity of radio receivers," RCA Rev. **6**, 332–344 (1942).
35. A. E. Burgess, R. F. Wagner, R. J. Jennings, and H. B. Barlow, "Efficiency of human visual signal discrimination," Science **214**, 93–94 (1981).
36. C. E. Bos and E. Deboer, "Masking and discrimination," J. Acoust. Soc. Am. **39**, 708–& (1966).
37. E. Eijkman, J. M. Thijssen, and A. J. Vendrik, "Weber's law, power law, and internal noise," J. Acoust. Soc. Am. **40**, 1164–1173 (1966).
38. W. M. Hartmann and J. Pumplin, "Noise power fluctuations and the masking of sine signals," J. Acoust. Soc. Am. **83**, 2277–2289 (1988).
39. L. E. Humes and W. Jesteadt, "Models of the additivity of masking," J. Acoust. Soc. Am. **85**, 1285–1294 (1989).
40. B. C. J. Moore, "Mechanisms of masking," J. Acoust. Soc. Am. **57**, 391–399 (1975).
41. E. Osman, "A correlation model of binaural masking level differences," J. Acoust. Soc. Am. **50**, 1494–1511 (1971).
42. V. M. Richards, L. M. Heller, and D. M. Green, "The detection of a tone added to a narrow band of noise: the energy model revisited," Q. J. Exp. Psychol. **43**, 481–501 (1991).
43. A. J. Ahumada, "Putting the visual system noise back in the picture," J. Opt. Soc. Am. A **4**, 2372–2378 (1987).
44. M. D'Zmura and K. Knoblauch, "Spectral bandwidths for the detection of color," Vision Res. **38**, 3117–3128 (1998).
45. K. R. Gegenfurtner and D. C. Kiper, "Contrast detection in luminance and chromatic noise," J. Opt. Soc. Am. A **9**, 1880–1888 (1992).
46. W. S. Geisler, "Sequential ideal-observer analysis of visual discriminations," Psychol. Rev. **96**, 267–314 (1989).
47. G. A. Hay and M. S. Chesters, "Signal-transfer functions in threshold and suprathreshold vision," J. Opt. Soc. Am. **62**, 990–998 (1972).
48. Z.-L. Lu and B. A. Dosher, "Characterizing the spatial-frequency sensitivity of perceptual templates," J. Opt. Soc. Am. A **18**, 2041–2053 (2001).
49. A. Rose, "The sensitivity performance of the human eye on an absolute scale," J. Opt. Soc. Am. A **38**, 196–208 (1948).
50. W. P. Tanner, Jr., and T. G. Birdsall, "Definitions of d' and n as psychophysical measures," J. Acoust. Soc. Am. **30**, 922–928 (1958).
51. B. S. Tjan, W. L. Braje, G. E. Legge, and D. Kersten, "Human efficiency for recognizing 3-D objects in luminance noise," Vision Res. **35**, 3053–3069 (1995).
52. A. Van Meeteren and H. B. Barlow, "The statistical efficiency for detecting sinusoidal modulation of average dot density in random figures," Vision Res. **21**, 765–777 (1981).
53. Z.-L. Lu and B. A. Dosher, "External noise distinguishes attention mechanisms," Vision Res. **38**, 1183–1198 (1998).
54. B. A. Dosher and Z.-L. Lu, "Mechanisms of perceptual attention in precuing of location," Vision Res. **40**, 1269–1292 (2000).
55. B. A. Dosher and Z.-L. Lu, "Noise exclusion in spatial attention," Psychol. Sci. **11**, 139–146 (2000).
56. D. G. Pelli, "Uncertainty explains many aspects of visual contrast detection and discrimination," J. Opt. Soc. Am. A **2**, 1508–1531 (1985).
57. J. Nachmias and R. V. Sansbury, "Grating contrast: discrimination may be better than detection," Vision Res. **14**, 1039–1042 (1974).
58. J. M. Foley and G. E. Legge, "Contrast detection and near-threshold discrimination in human vision," Vision Res. **21**, 1041–1053 (1981).
59. G. E. Legge and J. M. Foley, "Contrast masking in human vision," J. Opt. Soc. Am. **70**, 1458–1471 (1980).
60. S. A. Klein and D. M. Levi, "Hyperacuity thresholds of 1 sec: theoretical predictions and empirical validation," J. Opt. Soc. Am. A **2**, 1170–1190 (1985).
61. J. M. Foley, "Human luminance pattern-vision mechanisms: masking experiments require a new model," J. Opt. Soc. Am. A **11**, 1710–1719 (1994).
62. A. B. Watson and J. A. Solomon, "Model of visual contrast gain control and pattern masking," J. Opt. Soc. Am. A **14**, 2379–2391 (1997).
63. A. Gorea and D. Sagi, "Disentangling signal from noise in visual contrast discrimination," Nat. Neurosci. **4**, 1146–1150 (2001).
64. R. E. Fredericksen and R. F. Hess, "Temporal detection in human vision: Dependence on stimulus energy," J. Opt. Soc. Am. A **14**, 2557–2569 (1997).
65. L. L. Kontsevich, C. C. Chen, and C. W. Tyler, "Separating the effects of response nonlinearity and internal noise psychophysically," Vision Res. **42**, 1771–1784 (2002).
66. L. A. Olzak and J. P. Thomas, "Neural recoding in human pattern vision: model and mechanisms," Vision Res. **39**, 231–256 (1999).
67. L. Itti, J. Braun, and C. Koch, "Modelling the modulatory effect of attention on human spatial vision," in *Advances in Neural Information Processing Systems*, T. G. Ditterich, S. Becker, and Z. Ghahramani, eds. (MIT Press, 2002), pp. 1247–1254.
68. J. A. Solomon and M. J. Morgan, "Stochastic re-calibration: contextual effects on perceived tilt," Proc. R. Soc., London, Ser. B **273**, 2681–2686 (2006).
69. D. H. Brainard, "The Psychophysics Toolbox," Spatial Vis. **10**, 433–436 (1997).
70. X. Li, Z.-L. Lu, P. Xu, J. Jin, and Y. Zhou, "Generating high gray-level resolution monochrome displays with conventional computer graphics cards and color monitors," J. Neurosci. Methods **130**, 9–18 (2003).
71. Z. L. Lu and G. Sperling, "Second-order reversed phi," Percept. Psychophys. **61**, 1075–1088 (1999).

72. F. A. Wichmann and N. J. Hill, "The psychometric function: I. Fitting, sampling, and goodness of fit," Percept. Psychophys. **63**, 1293–1313 (2001).
73. JS could not perform better than 85% correct in the highest external noise condition in some of the orientation difference conditions. We excluded his data in that condition in all the analysis.
74. L. T. Maloney, "Confidence Intervals for the parameters of psychometric functions," Percept. Psychophys. **47**, 127–134 (1990).
75. D. P. Andrews, "Perception of contours in the central fovea," Nature **205**, 1218–1220 (1965).
76. W. S. Geisler, "Physical limits of acuity and hyperacuity," J. Opt. Soc. Am. A **1**, 775–782 (1984).
77. Dosher and Lu [54] (2000) showed that the stochastic *PTM* exhibits all the key characteristics derived for the simplified (analytic) *PTM*. In general, the analytic PTM is a close approximation to the stochastic *PTM* and provides a good approach to model testing: The (analytic) *PTM* fits all the data we have collected very well. In the special case when $\gamma = 1.0$, the (analytic) *PTM* is identical to the stochastic *PTM*. In the two extreme regions of the external noise manipulation, i. e., when internal additive noise dominates or when external noise dominates, the (analytic) *PTM* model approaches the stochastic model asymptotically.
78. In the *ePTM* development, the external noise in the stimulus had a Gaussian distribution, corresponding to white external noise. After nonlinear transduction, the distribution of the external noise might deviate from the Gaussian distribution. Spatial and temporal summation in the perceptual system should reduce this deviation. When combined with additive and multiplicative noises, both of which are Gaussian distributed, we assume that the sum of the noises is approximately Gaussian. However, we restrict ourselves to performance levels below 90% so as to avoid the tails of the distribution. The Gaussian assumption is not central to the development of the *PTM* outlined above, but it does simplify the application to signal detection estimation: the Gaussian noise distribution allows us to use the Gaussian form of signal detection calculations.
79. For a Gaussian random variable R with mean 0 and standard deviation $N_{ext}\sigma_{TN}$, the standard deviation of $sign(R)abs(R)^{\gamma_1}$ is $N_{ext}^{\gamma_1}\sigma_{TN}^{\gamma_1}F^{\gamma_1}(\gamma_1)\ldots F(\gamma_1)=1.00$, 1.07, 1.14, 1.20, 1.26, 1.32, 1.37, 1.42, 1.47, 1.52, and 1.57, for = 1.0, 1.2, …, 3.0.
80. B. A. Dosher and Z.-L. Lu, "Mechanisms of perceptual learning," Vision Res. **39**, 3197–3221 (1999).
81. Z.-L. Lu and B. A. Dosher, "Spatial attention: Different mechanisms for central and peripheral temporal precues?" J. Exp. Psychol. **26**, 1534–1548 (2000).
82. G. Westheimer and E. J. Ley, "Spatial and Temporal Integration of Signals in Foveal Line Orientation," J. Neurophysiol. **77**, 2677–2684 (1997).
83. This logic could be extended to consider more than two templates with an appropriate decision rule for identification tasks with more than two stimuli.
84. D. H. Parish and G. Sperling, "Object spatial frequencies, retinal spatial frequencies, noise, an the efficiency of letter discrimination," Vision Res. **31**, 1399–1415 (1991).
85. M. J. Morgan, "Hyperacuity," in *Spatial Vision*, D. Regan, ed. (CRC Press, 1991), pp. 87–113.
86. B. L. Beard and J. A. J. Ahumada, "Detection in fixed and random noise in foveal and parafoveal vision explained by template learning," J. Opt. Soc. Am. A **16**, 755–763 (1999).
87. B. A. Dosher, S.-H. Liu, N. Blair, and Z.-L. Lu, "The spatial window of the perceptual template and endogenous attention," Vision Res. **44**, 1257–1271 (2004).
88. A. Burgess, "Effect of quantization noise on visual signal detection in noisy images," J. Opt. Soc. Am. A **2**, 1424–1428 (1985).
89. J. A. Solomon and D. G. Pelli, "The visual filter mediating letter identification," Nature **369**, 395–397 (1994).
90. R. L. De Valois, E. William Yund, and N. Hepler, "The orientation and direction selectivity of cells in macaque visual cortex," Vision Res. **22**, 531–544 (1982).
91. D. H. Hubel and T. N. Wiesel, "Receptive fields, binocular interaction and functional architecture in the cat's visual cortex," J. Physiol. (London) **160**, 106–154 (1962).
92. A. Bradley, B. C. Skottun, I. Ohzawa, G. Sclar, and R. D. Freeman, "Visual orientation and spatial frequency discrimination: a comparison of single neurons and behavior," J. Neurophysiol. **57**, 755–772 (1987).
93. F. W. Campbell and J. J. Kulikowski, "Orientational selectivity of the human visual system," J. Physiol. (London) **187**, 437–445 (1966).
94. P. Makela, D. Whitaker, and J. Rovamo, "Modelling of orientation discrimination across the visual field," Vision Res. **33**, 723–730 (1993).
95. S. J. Waugh, D. M. Levi, and T. Carney, "Orientation, masking, and vernier acuity for line targets," Vision Res. **33**, 1619–1638 (1993).
96. G. Westheimer, "Visual hyperacuity," in *Progress in Sensory Physiology*, D. Ottoson, ed. (Springer, 1981), pp. 1–30.
97. J. Beck and T. Halloran, "Effects of spatial separation and retinal eccentricity on two-dot vernier acuity," Vision Res. **25**, 1105–1111 (1985).
98. D. Regan and K. I. Beverley, "Postadaptation orientation discrimination," J. Opt. Soc. Am. A **2**, 147–155 (1985).
99. G. Westheimer, K. Shimamura, and S. P. McKee, "Interference with line-orientation sensitivity," J. Opt. Soc. Am. **66**, 332–338 (1976).
100. H. R. Wilson and D. J. Gelb, "Modified line-element theory for spatial-frequency and width discrimination," J. Opt. Soc. Am. A **1**, 124–131 (1984).
101. H. R. Wilson and D. Regan, "Spatial-frequency adaptation and grating discrimination: predictions of a line-element model," J. Opt. Soc. Am. A **1**, 1091–1096 (1984).
102. R. Vogels and G. A. Orban, "How well do response changes of striate neurons signal differences in orientation: a study in the discriminating monkey," J. Neurosci. **10**, 3543–3558 (1990).